AT5

DESY 97-033
Baikal Note 97-01
February 1997

The Baikal Underwater Neutrino Telescope: Design, Performance and First Results

BAIKAL Collaboration

ISSN 0418-9833

DESY 97-033 ISSN 0418-9833
Baikal Note 97-01
February 1997

The Baikal Underwater Neutrino Telescope: Design, Performance and First Results

I.A.Belolaptikov[7], L.B.Bezrukov[1], B.A.Borisovets[1], N.M.Budnev[2], E.V.Bugaev[1], A.G.Chensky[2], I.A.Danilchenko[1], J.-A.M.Djilkibaev[1], V.I.Dobrynin[2], G.V.Domogatsky[1], L.A.Donskych[1], A.A.Doroshenko[1], G.N.Dudkin[6], V.Yu.Egorov[6], S.V.Fialkovsky[5], A.A.Garus[1], A.Gaponenko[2], A.V.Golikov[4], O.A.Gress[2], T.A.Gress[2], M.N.Gushtan[1], R.Heller[3], V.B.Kabikov[4], H.Heukenkamp[3], A.Karle[3], A.M.Klabukov[1], A.I.Klimov[9], S.I.Klimushin[1], A.P.Koshechkin[2], J.Krabi[3], V.F.Kulepov[5], L.A.Kuzmichov[4], O.Yu.Lanin[1], A.L.Lopin[2], B.K.Lubsandorzhiev[1], M.B.Milenin[5], T.Mikolajski[3], R.R.Mirgazov[2], A.V.Moroz[2], N.I.Moseiko[4], M.N.Nemchenko[2], S.A.Nikiforov[2], N.V.Ogievetsky[1], E.A.Osipova[4], A.N.Padusenko[6], A.I.Panfilov[1], Yu.V.Parfenov[2], A.A.Pavlov[2], D.P.Petukhov[1], K.A.Pocheikin[2], P.G.Pokhil[1], P.A.Pokolev[2], M.I.Rosanov[8], V.Yu.Rubzov[2], A.V.Rzhestshitski[2],S.I.Sinegovsky[2], I.A.Sokalski[1], Ch.Spiering[3], O.Streicher[3], A.A.Sumanov[1], L.Tanko[7], T.Thon[3], B.A.Tarashanski[2], I.I.Trofimenko[1], Ch.Wiebusch[3], R.Wischnewski[3],V.L.Zurbanov[2]

[1] *Institute for Nuclear Research, Russian Acad. of Science (Moscow, Russia),*
[2] *Irkutsk State University (Irkutsk, Russia),*
[3] *DESY Institute for High Energy Physics (Zeuthen, Germany)*
[4] *Moscow State University (Moscow, Russia),*
[5] *Nizhni Novgorod State Technical University (Nizhni Novgorod, Russia),*
[6] *Tomsk Polytechnical Institute (Tomsk, Russia)*
[7] *Joint Institute for Nuclear Research (Dubna, Russia),*
[8] *St.Petersburg State Marine Technical University (St.Petersburg, Russia),*
[9] *Kurchatov Institute (Moscow, Russia)*

Abstract

A first deep underwater detector for muons and neutrinos, *NT-200*, is currently under construction in Lake Baikal. Part of the detector, *NT-36*, with 36 photomultiplier tubes at three strings, has been installed in 1993. This array allowed for the first time a three-dimensional mapping of Cherenkov light deep underwater. Since then, various arrays have been almost continuously taking data. Presently a 96-PMT array is operating. We describe the *NT-200* detector design and present results obtained with *NT-36*.

Preprint submitted to Astroparticle Physics

1 Introduction

The spectrum of charged cosmic particles extends up to energies around 10^{11} GeV – far above any energy attainable with man-made particle accelerators. However, until now the cosmic world of high energies is essentially a *terra incognita* with respect to its sources. This is since the directional information of charged particles is washed out by their deflection in the galactic magnetic fields. Source tracing (i.e. *astronomy*) is possible only by neutral, stable particles pointing back to their origin, that means by γ-rays and by neutrinos. Unlike γ-rays which are absorbed by a few hundred grams/cm^2, neutrinos can escape regions of particle acceleration strongly shadowed by matter. In addition, neutrinos of any energy can reach us from the most distant parts of the observable Universe, whereas γ-rays of TeV energy and beyond are absorbed by interstellar light. On the other hand, the weakness of neutrino interactions makes detection much more difficult than in the case of γ-rays and requires huge detectors.

High energy neutrinos in the TeV range can be inferred easiest from upward traveling muons produced in charged current ν_μ interactions in rock or water close to the detector. With the angle between parent neutrino and muon being approximately $1.5^o \cdot E_\nu^{-0.5}$ [TeV], astronomy with degree resolution is possible in the TeV region. The main parameter characterizing the detection capability with respect to high energy muon neutrinos is the detector *area*, or, for deep underwater detectors, which actually see beyond their geometrical limits, the *effective area*. The perspective of scales larger than those attainable with underground detectors led to the idea [1] and later to the first project [2] of an under*water* neutrino telescope. These telescopes consist of a lattice of photomultipliers (PMTs) spread over a large open volume in the ocean or in a lake. The direction of the muon is inferred from the measured arrival times and amplitudes of the Cherenkov photons which are radiated by the muon and the accompanying electromagnetic shower particles. Technologies for underwater telescopes have been pioneered by the Baikal collaboration [3] and by the DUMAND project near Hawaii [4]. In the mean time, two underwater/ice detectors are taking data: the Baikal telescope and the AMANDA telescope the South Pole [5]. Also, the projects NESTOR [6] and ANTARES [7] in the Mediterranean have joined the efforts towards an underwater neutrino telescope.

The scientific goals of underwater telescopes are manifold. The basic motivation is to do high energy neutrino astronomy. Most favored candidates for particle acceleration are Active Galactic Nuclei (AGN) presumably powered by supermassive black holes at their center. Recent observations of TeV photons from close AGN [8] as well as AGN models [9] have been used to set the scale of 0.1-1 km^2 to identify neutrinos from these objects. Among possible sources in our galaxy, young pulsars may yield fluxes detectable with even smaller telescopes [10]. Another challenge is to check whether Gamma Ray Bursts, one of astronomy's top enigmas, emit part of their energy in neutrinos [11].

Beyond the field of neutrino astronomy, the diverse scientific missions of underwater telescopes include the search for neutrinos emerging from the annihilation of Weakly Interacting Massive Particles (WIMPs) in the center of the Earth or the sun (see e.g. [12, 13]), the search for neutrino oscillations, or for slowly moving, bright particles like GUT magnetic monopoles. They can contribute to such different fields like atmospheric muon physics on the one hand and – for a lake-based telescope – limnology on the other hand.

The possibility to build a neutrino telescope in Lake Baikal was investigated since 1980, with the basic idea [14] to use – instead of a ship – the winter ice cover of the lake as a platform for assembly and deployment of instruments. After first small size tests, in 1984 a first stationary *string* equipped with up to 12 photomultipliers of moderate size and time resolution was deployed and operated via a shore cable [3]. Strings with up to 36 PMTs were operated between 1986 and 1990 [15]. The main physics results obtained from these experiments are stringent upper limits on the flux of GUT magnetic monopoles catalyzing baryon decay [16]. On the methodical side, underwater and ice technologies were developed, particularly those for reliable deployment and retrieval of instruments. Also, water parameters were investigated in detail.

Since 1987, a "second generation experiment" with the capability to identify muons from neutrino interactions was envisaged. According to the number of PMTs, this detector was named *NT-200* (Neutrino Telescope with $\approx$ 200 PMTs [15]). With an effective area of about 2000 m^2 for 1-TeV muons, it is a first stage of a future large telescope which will be built stepwise, gaining experience with detectors of rising size and complexity.

Tailored to the needs of the Baikal experiment, a large area hybrid phototube *QUASAR-370* [17] with a time resolution of better than 3 nsec was developed. Small test strings with 8 and 14 *QUASARs* have been operated in 1991 and 1992, respectively [19]. In 1993, a first multistring array, *NT-36*, was deployed. 36 PMTs mounted on 3 different strings allowed, for the first time, a three-dimensional reconstruction of muon tracks deep underwater. The results presented in this paper are mainly based on the data taken with *NT-36* from April 1993 to March 1994. A modified array, *NT-36'* came into operation in April 1994. It was replaced by a 72-PMT array one year later. Presently, *NT-96*, a four-string array with 96 PMTs is taking data in Lake Baikal.

The present paper aims to summarize the experience gained with *NT-36*, to present first physics results and to draw conclusions with respect to future large telescopes. The paper is organized as follows:

Section 2 summarizes the optical parameters at the site of the Baikal experiment and describes the mechanical construction and the functional design of *NT-200*. In sections 3 to 6, results obtained with *NT-36* are described. Section 3 summarizes the main parameters of *NT-36* and discusses the observed time variations of trigger rates. In section 4, the reconstruction of muon tracks is elaborated, whereas section 5 focuses on the capabilities of the Baikal detector to identify upward moving muons from neutrino interactions. Section 6 is devoted to the search for magnetic monopoles. Section 7 presents the conclusions and sketches possible future routes of development of the Baikal Neutrino Telescope.

2 The Design of the Detector

2.1 Site and optical parameters of the water

The Baikal Neutrino Telescope is being deployed in the Southern part of Lake Baikal (see fig.1). The geographical coordinates of the detector site are $51°50'N$ and $104°20'E$, the distance to shore is 3.6 km. The depth of the lake is 1366 m at this location.

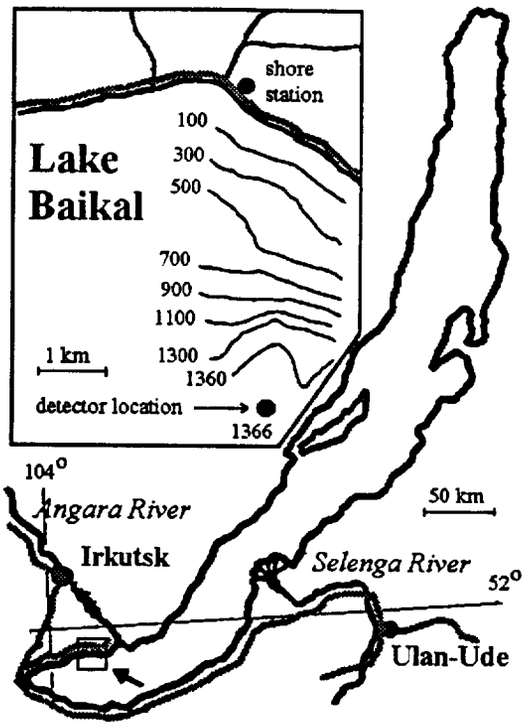

Figure 1: Site of the Baikal experiment

The optical parameters of the water at the depth of the detector (about 1100 m) have been measured with special instruments and with the telescope itself over many years [18, 20, 15, 21, 22, 23]. The main results of these measurements are:

1. The absorption length L_{abs} for wavelengths λ between 470 and 500 nm is about 20 m; seasonal variations typically are less than 20 %.

2. Light scattering is strongly anisotropic. The mean cosine of the scattering angle θ from measurements covering the angle interval 2° to 100° is close to 0.95. The scattering length L_{scatt} shows strong seasonal variations. Typical values are about 15 m, i.e. close to the absorption length. The maximum value measured is 23 m, but also 7 m have been reported. Sometimes [24] the so-called effective scattering length $L_{eff} = L_{scatt}/(1 - \langle\cos\theta\rangle)$ is used to characterize the relative merits of different sites for neutrino telescopes. With L_{scatt}= 15 m and $\langle\cos\theta\rangle) = 0.95$ one obtains $L_{eff} = 300$ m for the Baikal site.

3. The water luminescence shows strong seasonal variations, with typical values of 25 counts per second and cm^2 photocathode. This is of the same order of magnitude as the light level from K^{40} decays in Oceans [25]. The variations of the counting rates due to water luminescence allow to investigate limnological questions like the seasonal change of water currents. From the rate variations measured in 1993 and 1994 conclusions can been drawn with respect to the deep water ventilation in Lake Baikal.

Fig.2 shows the absorption coefficient $\kappa = 1/\lambda_{abs}$ and the scattering coefficient $\sigma = 1/\lambda_{scatt}$ as function of the wavelength, measured in autumn 1993 at a depth of 1100 m.

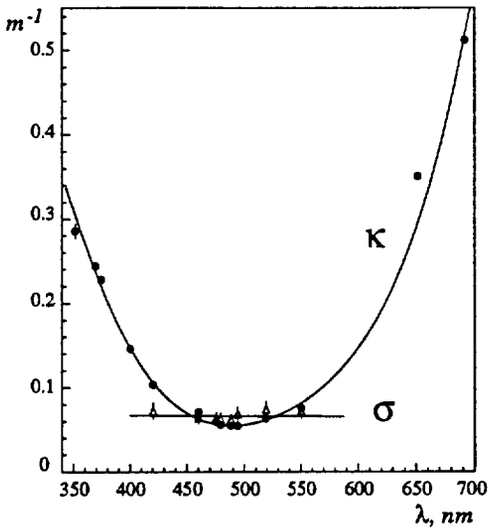

Figure 2: Coefficients for light absorption (κ) (dots) and scattering (σ) (triangles) at the site of the Baikal Neutrino Telescope as a function of wavelength. Date of measurement: Oct./Nov.1993. Depth: 1100 m.

2.2 Deployment and mechanical construction of the detector

Fig.3 sketches the present instrumentation of the site. The basic structural elements of the complex are *strings*. The strings are anchored by weights at the bottom of the lake, and held in a vertical position by buoys at various depths. The upper buoy is located at a depth of 20 m below the surface. The deployment of the detector is carried out during a 5 to 7 week period in late winter, when the lake is covered by a thick layer of ice. A string is retrieved by catching its upper buoy and winching it to the ice surface. Three cables (*1,2,3* in fig.3) connect the detector site with the shore station. The cables are layed during winter through a slit cut in the ice from the site of the detector to the shore. Each shore cable ends at the top of a string (*4,5,6*, respectively). The strings are connected by horizontal cables fixed just below the upper boys. All connection operations can be done on ice [26].

String *7* carries the telescope. A special "hydrometric" string (*8*) at a distance of 120 m from the telescope is equipped with instruments to measure the optical parameters of the water, as well as water currents, temperature, pressure and sound velocity. The spatial coordinates of the components of the telescope are monitored by a hydroacoustical system. The signals from several battery-powered ultrasonic emitters (*9-14*) placed at radial distances of 600 m from the telescope are registered by receivers fixed at the bottom and at the top of each of the strings of the telescope. The displacements of the whole array due to water currents have been measured to be smaller than 2 m, the relative positions of the optical modules change by less than the OM diameter [27].

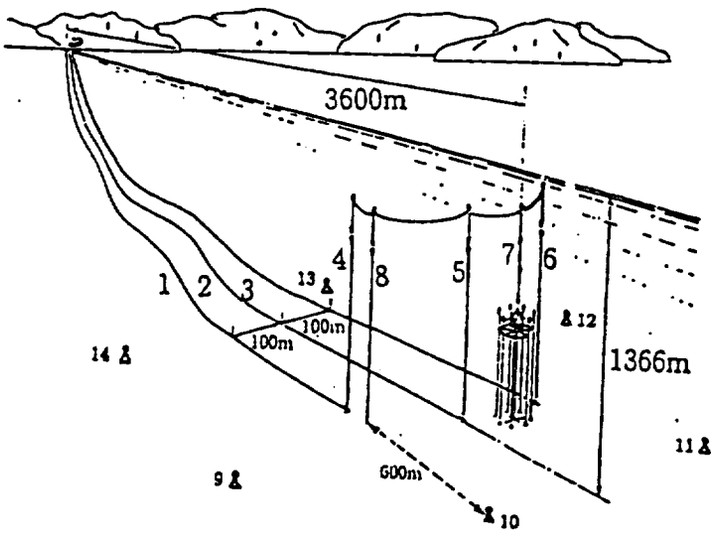

Figure 3: The Baikal detector complex (status since 1994). *1,2* – wire cables to shore, *3* – opto-electrical cable to shore, *4,5,6* – string stations for shore cables 1,2,3, respectively, *7* – string with the telescope, *8* – hydrometric string, *9-14* – ultrasonic emitters

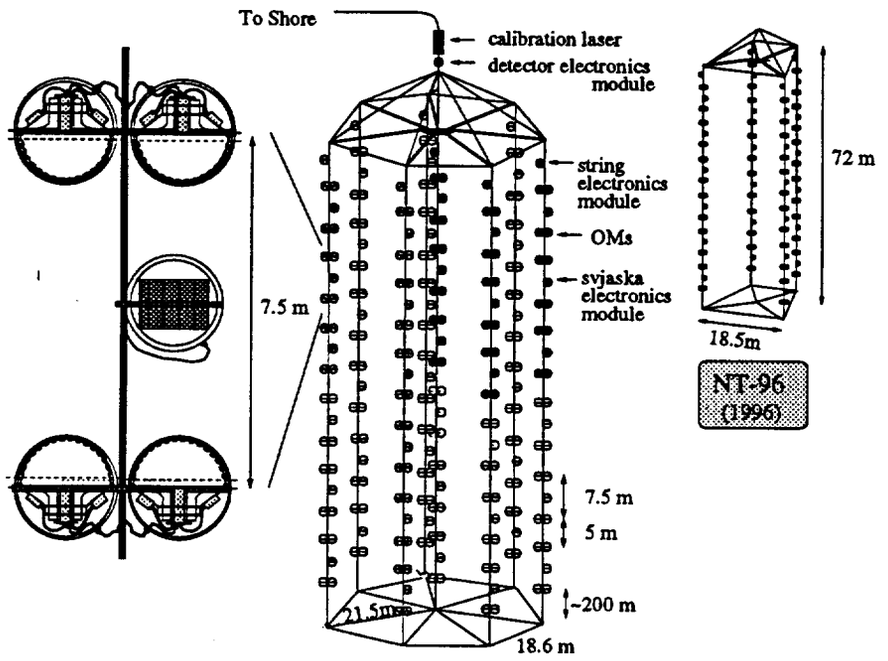

Figure 4: Schematic view of the Baikal Telescope *NT-200*. The modules of *NT-36*, operating 1993/94 are in black, the modules added in 1995 are in grey. The expansion left-hand shows 2 pairs of optical modules ("svjaska") with the svjaska electronics module, which houses parts of the read-out and control electronics. Top right the array *NT-96* is shown, which has been deployed in 1996.

Mechanically, *NT-200* consists of 8 strings arranged at the edge and at the center of an equilateral heptagon (fig.4). The strings are attached to a rigid frame consisting of 7 arms each 21.5 m in length. The system is balanced by a sophisticated system of horizontal and slanted ropes (partly indicated in fig.4) and buoys. In order to retrieve a string with failed elements or to mount a new one, the whole system is pulled up. Then, through a hole approximately above the string position, the corresponing arm is inclined and the string is mounted/dismounted. Again, no electrical connections have to be done under water. The combination of easy retrieval and avoiding connections to be mounted underwater distinguishes the Baikal project from the other underwater/ice projects [5, 4, 6, 7].

The optical modules (OMs) are grouped in pairs along the strings. In the original design [15], and also for *NT-36*, they are directed alternatingly upward and downward. The distance between pairs looking face to face is 7.5 m, while pairs arranged back to back are 5 m apart. The up/down symmetry of the array facilitated a study of the array performance using downward-going muons. In the case of the 1995 detector *NT-96*, most modules point down - firstly in order to increase the effective area for upward muons and secondly to reduce the deterioration of the array due to sedimentation effects (see section 3.2).

2.3 The Optical Module

The OM [30] consists of a pressure tight glass sphere housing the phototube as well as several electronic components. A detailed description will be published elsewhere [31].

The 37 cm diameter phototube *QUASAR-370* [32, 17] consists of an electro-optical preamplifier followed by a conventional photomultiplier (PMT) - see fig.5. Photoelectrons from a large hemispherical photocatode covering nearly 2π are accelerated by 20-25 kV to a fast, high gain scintillator (Y_2SiO_5:Ce) which is placed near the center of the glass bulb. The light from the scintillator is read out by a small conventional PMT (*"UGON"*). The high gain of the electro-optical preamplifier results in an excellent single photoelectron resolution of 70% and a peak-to-valley ratio of 2.5. The time jitter is typically 3 nsec for 1 p.e. full photocathode illumination. The tube is almost insensitive to the earths magnetic field.

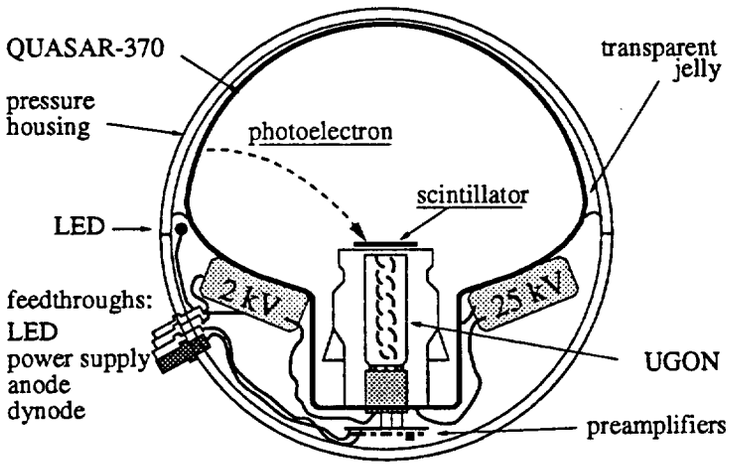

Figure 5: The Optical Module of the Baikal experiment (see text for explanations)

Apart from the *QUASAR*, the OM contains the high voltage supplies yielding 25 kV for the electro-optical amplifier and 1.6 to 2.3 kV for the conventional PMT, a LED with driver for test and calibration of the *QUASAR*, and preamplifiers for the signal from the next-to-the-last dynode and the anode. The OM is equipped with 4 hermetic feed-throughs. Signals from anode and dynode are read out via 2 of the cables, the 3rd cable transmits the supply voltage, the LED is controlled via the 4th cable.

2.4 Front-end electronics, trigger formation and data acquisition

The two PMTs of a pair are operated in coincidence and define a *channel*. The coincidence window has a width of 15 nsec. At a threshold of 0.3 photoelectrons (p.e.), the typical counting rate due to noise and bioluminescence is 100 kHz for a single *QUASAR*. By the coincidence, the rate is reduced to 300 Hz per pair. This low counting rate is not only of significant advantage for underwater triggering and data transmission, but also leads to events nearly free of random hits. The latter fact is essential for the difficult task of track reconstruction [31, 40].

The coincidence is formed in the *svjaska* electronics module. Two PMT pairs are connected to one of these modules (see fig.4). Fig.6 shows the circuitry in the svjaska electronics module for *one* pair. The anode signals are sent to discriminators and then switched in pairwise coincidence. The discriminator thresholds are set remotely controllable to values between 0.25 and 0.5 p.e. The dynode signals are sent to a *Q-T* converter. The length of its output signal corresponds to the charge of the dynode signal, the leading edge defines the time information and is set by the earliest of the two discriminator output signals.

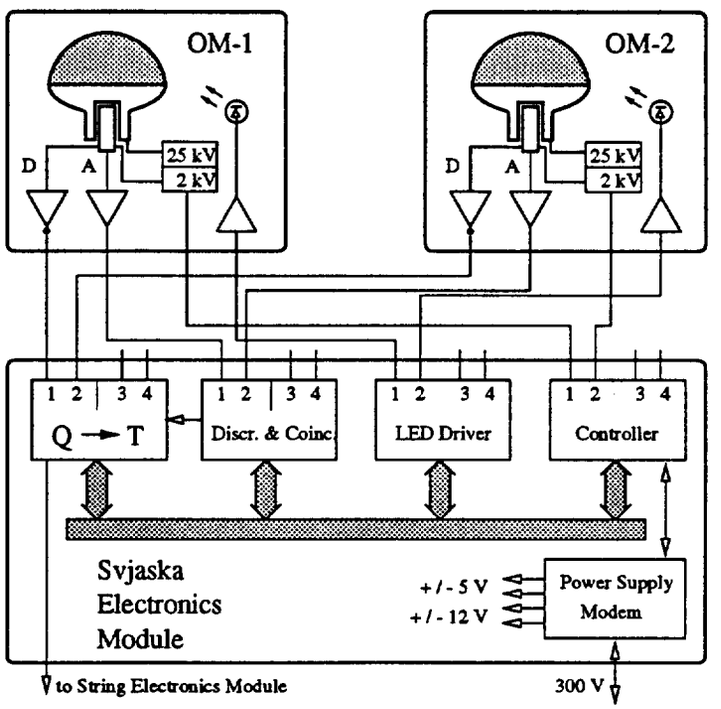

Figure 6: Scheme of the svjaska electronics controlling 2 pairs of OMs (only the 2 PMTs belonging to the first pair are shown).

Further components housed in the svjaska electronics module are the LED driver and a Intel8085-based micro-computer which controls HV, discriminator thresholds and the LED regime. In order to monitor the performance of the OMs, the counting rates of individual PMTs as well as of the channels are measured and transmitted to shore once per 30-60 sec. The micro-computer is controlled from shore.

The next stage in the system hierarchy are the *string* electronics modules, one for 6 channels (see fig.4). They contain TDCs which digitize the time (11 bit) and the amplitude (10 bit) information carried by the Q-T converted signal from each channel. The dynamical range of the amplitude system is ≈ 1000 p.e., with a resolution of 1 p.e., an additional mode used for calibration has a range of 30 p.e. The time digitization system has a resolution of 1 nsec.

Stability of the digitization is checked by calibration runs performed typically once every two days. The calibration of the relative time shifts between all channels is performed with the help of a nitrogen laser of 300 psec pulse width positioned above the array (see fig.4). The light from this laser is guided by optical fibers of equal length separately to each OM pair.

The formation of the muon trigger is sketched in fig.7. In case of a coincidence of the two PMTs of a pair (*local trigger*), a request signal of 600 nsec length is sent to the *detector* (central) electronics module fixed at the top of the heptagon. There, the summed signals from six channels each are fed to an analog summator building the overall sum. The summators output is led to a discriminator. A *muon trigger* is formed by the requirement of $\geq m$ local triggers within a time window of 500 nsec (this is about twice the time a relativistic particle needs to cross the *NT-200* array). The threshold value m of the discriminator can be set from shore to values between 1 and 7, typical thresholds are 3 and 4.

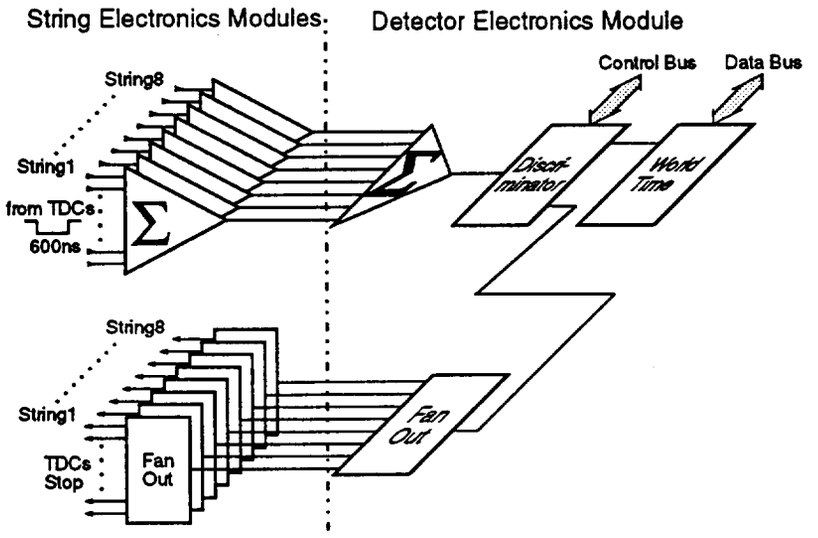

Figure 7: Formation of the muon trigger.

Once a muon trigger is formed, the amplitude and time digitizations, already initialized in the string electronics modules, are completed. In addition to the channels having generated the muon trigger, also all local triggers within a time window of -1.0μsec to +0.8μsec with respect

to the muon trigger signal are recorded. The string electronics adds an event number to the ADC and TDC information from each hit channel and transmits this information to the detector electronics module.

In the detector electronics module, the data words from each local trigger are complemented by an event number and a time counter with 10 μsec step which relates the internal event time to the local ("world") time. From here the information is sent to shore.

The data acquisition system in the shore station is based on a robust and almost maintenance free configuration consisting of three PCs and and a transputer network [33]. Fast data-preprocessing and on-line histogramming is done on the transputer system before data are stored on the main PC. This PC is also connected to the controllers in the svjaska, string and detector electronics modules (slow control system). A "Monitor PC" allows on-line inspection of more than 600 histograms. The third PC controls the position monitor system, the power supply, and the instruments at the hydrological string.

Fig.8 sketches the structure of the DAQ system.

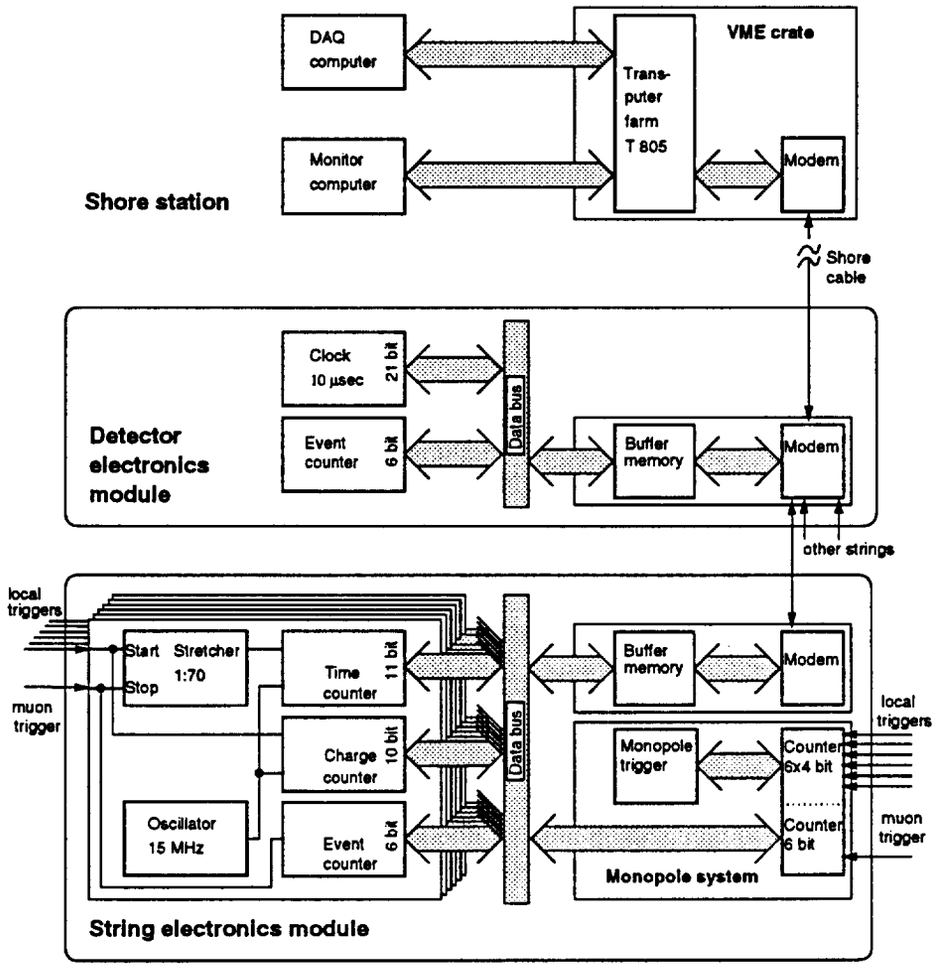

Figure 8: Scheme of the NT-200 data acquisition system

The muon trigger system described above is tailored to events caused by the passage of a relativistic particle. A second system searches for time patterns characteristic for slowly moving bright particles like nuclearities or GUT magnetic monopoles catalyzing proton decays. Depending on the velocity of the object, such events could cause enhanced counting rates in individual channels during time intervals of 0.1 – 0.8 msec, separable from Poissonian noise.

The monopole system is based on XILINX Field Programmable Logic Arrays. It fetches the local trigger request signals into separate 4-bit counters. The time gate ΔT of the counters is programmable in 8 steps from 100 to 800 μsec or, for test purposes, from 1 msec to to 8 msec. After ΔT elapsed, all counters are checked for contents exceeding a common threshold N (programmable from 1 to 7). If at least one of each six counters had yield $\geq N$ counts, the contents of all six counters are written into a data register. This information is complemented by the content of a 24 bit counter which is incremented every 100 μsec and serves as a time reference marker. A 6-bit counter incremented by the muon trigger allows to relate monopole triggers to muon events.

3 NT-36

3.1 Configuration and statistics

The array *NT-36* (see the modules marked black in fig.4) started data taking at April 13th, 1993, and was operated up to March 1994. There have been 6 PMT pairs along each of the 3 strings of *NT-36*. The orientation of the channels *1-6* was (from top to bottom): *down-up-down-up-down-up*. To optimize the performance of this sub-detector of *NT-200*, the arms of the heptagonal frame were inclined, resulting in a decreased distance of 15.5 m between central and peripheral strings.

For trigger *6/3* (i.e. $\geq$ 6 hits at 3 strings), suitable for three dimensional track reconstruction, the effective area of *NT-36* is calculated to be 150 m^2 for atmospheric muons (threshold 10 GeV). It rises with energy to 270 m^2 for 1 TeV muons and to 1000 m^2 for 10 TeV muons.

The main muon data taking runs were interrupted only due to calibration runs, operation of the environmental units, power failures and thunderstorms. During 176.2 days of data taking, $4.53 \cdot 10^7$ events for the basic trigger *3/1* ($\geq$ 3 hits at $\geq$ 1 string) have been taken (10 Hz, when all 18 channels had been operational). In addition, $1.86 \cdot 10^7$ events have been recorded setting the trigger *4/1* and $5.3 \cdot 10^5$ setting *2/1*. Just before the 1993 array was pulled up (March 1994), 23 of the 36 individual Optical Modules were still in operation. Nine OMs were dead and 4 were not accessible due to a failure of a svjaska controller module. Altogether, 9 out of the originally 18 channels were still in operation. Losses have been due to failures of electronic components. All *QUASAR-370* turned out to be still operational. None of the pressure housings had leaked.

Unless specified otherwise, the results presented in this paper are obtained from the data taken with *NT-36* when $\geq$ 16 channels have been operating ($2.7 \cdot 10^6$ events for trigger 6/3). Preliminary results from *NT-36* have been presented first in [34, 35, 40].

3.2 Counting rates

For standard muon runs, the trigger condition was set to *3/1* or *4/1*. For 18 channels operating, the trigger rate was measured to be (10.01±0.02) Hz for the condition *3/1*, falling to (1.13±0.24)·10^{-3} Hz for events with all channels hit (*18/1*). For trigger *6/3*, used to select reconstructible events, the rate was (2.79 ± 0.01) Hz.

Counting rates of individual channels ("local trigger rates") are dominated by water luminescence. From August until mid-September we observed an increase of the luminosity to extremely high levels – sometimes the local trigger rates reached 2-2.5 kHz instead of typically 200-300 Hz. At the end of September, the counting rates smoothly approached their original level. The changes of the local trigger rate are not reflected in the muon trigger rate, since the muon trigger is essentially dominated by atmospheric muons, with negligible contribution by random hits (water luminescence or dark noise). This is demonstrated in fig.9 for a time interval of marked changes of the local trigger rate following a strong storm at August 3rd, 1993. In spite of the sharp increase of local triggers, no significant changes are observed in the muon trigger rate.

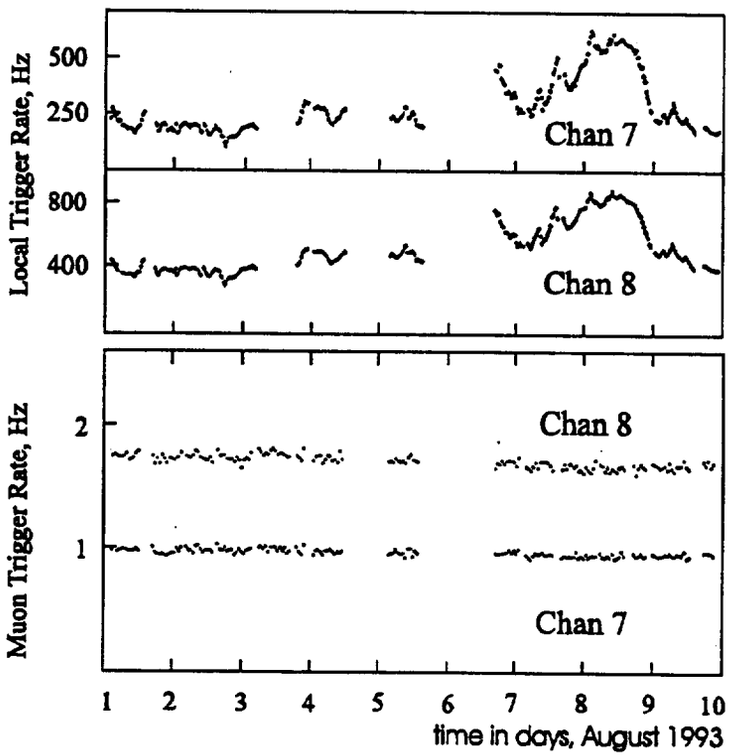

Figure 9: a) Local trigger rates for channel 7 (downward facing) and channel 8 (upward facing) for August 1st-9th, 1993. The counting rates are averaged over 30 min. b) Muon trigger rates (condition *4/1*) for channel 7 and 8. Counting rates are averaged over 50 min.

A phenomenon strongly influencing the sensitivity and, consequently, the counting rates of upward facing modules, is sedimentation of biomatter and dust on the upper hemispheres of the modules.

Fig.10 shows the trigger rates for two different conditions over a period of 225 days, starting with April 13th, 1993. Firstly, for the case that at least 4 upward facing channels have been hit (upper graph), secondly, for the condition that at least 4 downward facing channels have been hit (lower graph). Only channels operating all 225 days have been included. In the second case, one observes a slight decrease of the rates down to 85-90% of its original value. In contrast, the rate for the *upward* trigger falls down by nearly an order of magnitude.

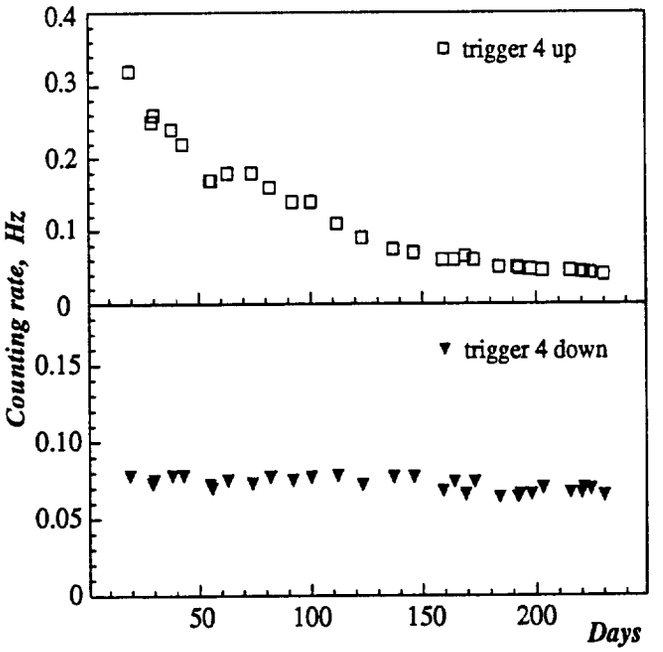

Figure 10: Trigger rates over a period of 225 days starting with April 13th, 1993. Top: condition *4-up* (at least 4 upward channels hit). Bottom: condition *4-down* (at least 4 downward channels hit).

The inspection of the spheres after one year of operation showed that sediments had formed a "hat" of bad transmission on the upward facing hemispheres. The region near the equator was nearly free of sediments. This suggests to describe the variation of the sensitivity η of an optical module by the following formula [31]:

$$\eta = \eta_0 \cdot (p_1 + (1 - p_1) \cdot e^{-t/p_2})$$

where t is the time after deployment in days. p_1 stands for the part of the sensitivity contributed by the equatorial region, the second term describes the top region with exponentially decreasing light transmission.

Replacing the sensitivity η_0 used in the Monte-Carlo calculations by η as defined above, and fitting the resulting trigger rates to those experimentally measured in 1993 (1994), one gets $p_1 = 0.33$ (0.36) and $p_2 = 96.2$ (102.0) days (numbers in brackets are for the 1994 array NT-36′). Consequently, the sensitivity of an upward facing module to atmospheric muons decreases to 35% after a year. Both parameters change only slightly from year to year. Note that the sensitivity of an upward facing OM to upward going muons from neutrino interactions might be

influenced only slightly, since for these tracks the equatorial part of the module is illuminated stronger than the top region. Presently, we are looking for methods to reduce sedimentation effects. E.g., the accumulation of sediments can be reduced by a smoother OM surface or by dressing the OM with a tapering plexiglas hat. In the presently operating array *NT-96* most of the OMs face downward.

4 Analysis of muon events

4.1 Monte Carlo event generation

In the following, experimental data are compared to predictions obtained by modeling the the main source of events registered with *NT-36*, namely atmospheric muons generated in the atmosphere above the array and punching through to the detector depth.

To generate atmospheric muons, a program developed by the Baksan group [36] was used. It generates proton interactions in the atmosphere and tracks showers down to muons at sea level. Stochastical energy loss, light propagation and detector response have been calculated with the Standard Monte Carlo package of the Baikal collaboration. Energy losses along the muon track smaller than 20 MeV are treated as continuous losses. In addition, for every energy loss above 20 MeV, the energy, the type and the direction of the particle(s) produced are stored in a stack; one entry for every interaction along the muon trajectory. This information is related to a library containing light fields as a function of the mentioned parameters. Photon fluxes from each individual interaction at the position of every OM are calculated using the measured absorption coefficient $\kappa(\lambda)$. Light scattering is not implemented in this Monte Carlo version. From the photon flux, the mean amplitude is calculated, taking into account the measured sensitivity of the OM as well as its sensitive area pointing into the direction of the light source, and summing over the light from all sources along the muon track. The time information is given by the signal from the first photoelectron exceeding the amplitude threshold in one of the two OMs of a channel. The PMT jitter was parametrized convoluting an exponential jitter with $\tau = 4\ \mathrm{nsec}/N_{pe}$ and a fixed Gaussian jitter with $\sigma = 1.6$ nsec. Dark noise signals or random photons hitting an OM just before the arrival of a photon emitted by a muon cause dead time effects on a few percent level. These effects are taken into account using the continuously monitored counting rates of individual PMTs and of channels.

4.2 Timing characteristics

Fig. 11 illustrates the performance of the laser time calibration system. The arrival times of the laser pulses, guided through fibers of equal length to the OMs, measure the relative time shift between all channels. The figure shows the distribution of time differences $\Delta t_{i,j} = t_i - t_j$ between light arrival times t_i and t_j at channels i and j, respectively. It shows a narrow peak at zero for the laser pulses and a broad distribution for muonic events peaking at a value characteristic for the distance between the channels selected ($\Delta t \approx 83$ nsec for $\Delta x = 25$ m). The width of the laser peak (FWHM ≈ 2 nsec) gives an estimate of the time resolution of the whole system for large

amplitudes ($A \approx 50$ p.e.). For much smaller amplitudes, the PMT jitter would be dominant. The laser is also used to measure the detection inefficiency of the individual channels, which is typically 2-5% and is caused by dead time effects.

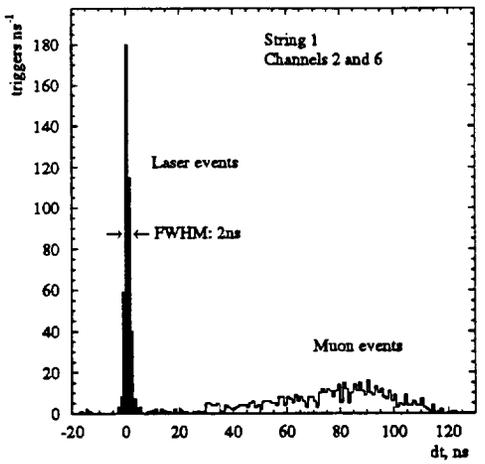

Figure 11: Distribution of light arrival time differences $\Delta t_{i,j,} = t_j - t_i$ for channels 2 and 6 (string 1) for a typical laser run, with muon triggers recorded in parallel.

The distribution of light arrival time differences for muon runs is illustrated in fig. 12 (channels 10 and 12 on string 2). One finds a dominant peak around $\Delta t_{10,12} = 37.1$ nsec. It is essentially due to muons, as proved by the Monte Carlo curve (dashed line). The almost flat parts of the experimental distribution ranging up to ≈ -1000 nsec and $+1000$ nsec originate from random non-muon hits in the muon trigger time window (500 nsec) as well as in the larger window considered once a trigger has been formed (see section 2.4).

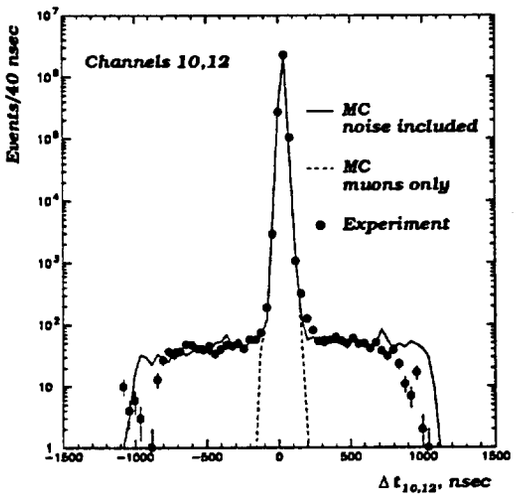

Figure 12: Distribution of light arrival time differences $\Delta t_{i,j,} = t_j - t_i$ for channel 10 and 12 (string 2) for a muon run with trigger *4/1*. Points are experimental data, lines are MC results without noise (dashed line) and with noise due to random hits (full line).

For 100 Hz local counting rates, we expect a noise contribution of the order of 10^{-4} per channel per muon trigger. The quantitative behavior of the noise contribution is well reproduced by the MC curve once noise hits according to the true local counting rates are included (full curve in fig.12).

From fig.12, we determine the rate of noise hits to $1.01 \cdot 10^{-4}$ per channel per event for the full time window. For the restricted $\Delta t_{i,j}$ interval within the muon peak ($-50...150$ nsec), the noise rate is reduced to $0.11 \cdot 10^{-4}$. From that, the noise contribution per event from *all* channels and for trigger 4/1 is obtained to be about $2 \cdot 10^{-3}$ for *NT-36* and $1 \cdot 10^{-2}$ for *NT-200.*

Fig.13 shows the distribution of light arrival time differences, $\Delta t_{i,j}$, for different channel combinations on a zoomed, linear scale. Monte Carlo and experiment are found to coincide quite well for most channels. However, there are combinations showing deviations mostly due to electronic defects which have been partly eliminated in the mean time.

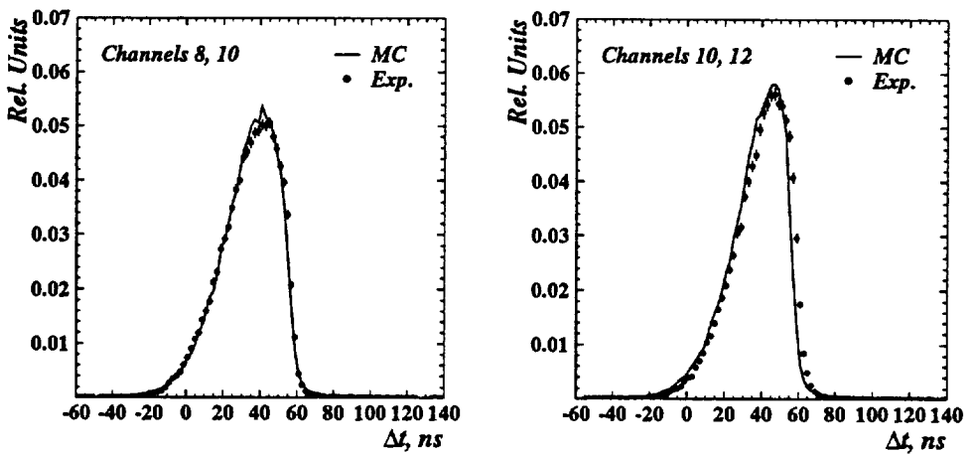

Figure 13: Distribution of light arrival time differences $\Delta t_{i,j} = t_j - t_i$ for different channel combinations. Points are experimental data, MC results are given by the solid line.

4.3 Amplitude characteristics

Fig. 14 shows the amplitude distributions for channels 7 and 8. The good agreement between MC and experiment is only obtained by correctly modeling of the effects of δ-electrons and showers accompanying the muon. Monte Carlo calculations show that 66 % of all events in *NT-36* fulfilling the condition *5/3* are due to single muons, in 34 % the event includes hits from several muons ("muon bundles"). 88 % of the single muons are accompanied by at least one shower with an energy release greater than 20 MeV, in 24 % the largest shower releases even more than 10 GeV.

A high dynamic range and a good linearity of amplitude measurements are essential in order to estimate the energy of muons from the light they emit. As has been shown in [15] for *NT-200*, in the multi-TeV region the resolution in $\ln E_\mu$ is about 0.5, i.e., it is possible to determine the order of magnitude of the muon energy.

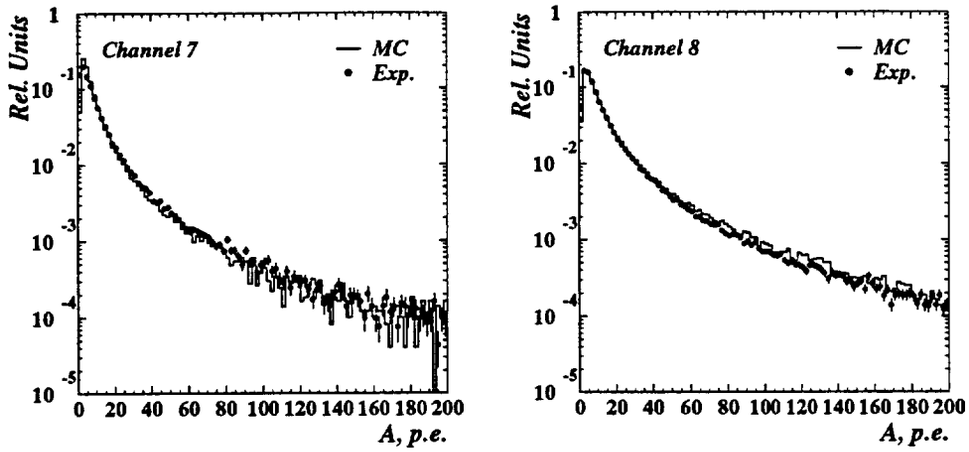

Figure 14: Distribution of the amplitudes for channel 7 and 8. Points: experimental data, solid line: muons including full energy loss.

4.4 Reconstruction of atmospheric muons

The reconstruction of the track parameters of a particle crossing a deep underwater telescope turns out to be complicated compared to typical under*ground* detectors. There, the track is either well defined by scintillators or gaseous track detectors [37, 38], or it is given by the hit pattern and arrival times of PMTs covering the inner surface of a water volume with a rather fine lattice [39]. In underwater detectors, the PMT lattice is spanned over the telescope volume with a very large spacing. The large spacing increases – for a given number of PMTs – the effective area; on the other hand it also increases the energy threshold of the array and, most important in our context, results in a lower degree of redundancy compared to underground detectors.

The parameters of a single muon track can be determined by minimizing

$$\chi_t^2 = \sum_{i=1}^{N_{hit}} (T_i(\theta, \phi, u_0, v_0, t_0) - t_i)^2 / \sigma_{ti}^2$$

Here, t_i are the measured times and T_i the times expected for a given set of track parameters. N_{hit} is the number of hit channels, σ_{ti} are the timing errors. A set of parameters defining a straight track is given by θ and ϕ – zenith and azimuth angle of the track, respectively, u_0 and v_0 – the two coordinates of the track point closest to the center of the detector, and t_0 – the time the muon passes this point. By setting $\delta S_t^2/\delta t = 0$ and solving for t_0, an analytical solution for the time parameter can be found. This reduces the parameter space to be searched for a χ^2 minimum from five to four dimensions.

We did not include an amplitude term χ_a^2 analog to χ_t^2 in the present analysis, but used the amplitude information only to calculate the timing errors σ_{ti} in the denominator of the formula above.

By various reasons, the result of the fit can deviate considerably from the true parameters of the trajectory. Firstly, χ_t^2 has a complicated behavior, characterized in many cases by several local minima. Secondly, there are often several true minima which reflect internal symmetries of the detector not resolvable by timing information alone. Thirdly, it often happens that a large fraction of the hit PMTs detect only light from electromagnetic showers and not from the muon itself. Since photons from showers are generally delayed compared to directly emitted photons, and since they have a different angular distribution, the picture of a "naked" muon fails. The situation may be further complicated by photons delayed due to light scattering in water.

We adopted the following reconstruction procedure [40]:

- Application of several causality criteria rejecting events which violate the model of a naked muon and a 0-th approximation of θ and ϕ.
- A χ^2 minimum search, using the model of a naked muon and only time information.
- Quality criteria to reject most badly reconstructed events.

The causality criteria refer to time differences between channels. For instance, one requests that each combination of two channels i, j obeys the condition $c\,|dt_{ij}| < n\,|dx_{ij}| + \delta t$. The term $\delta t =$ 5 nsec accounts for time jitter and shower events, n denotes the index of refraction of water.

Some of the most effective quality criteria are upper limits on parameters like the minimum χ^2; the product of probabilities P_{nohit} of non-fired channels not to respond to a naked muon and of probabilities P_{hit} of fired channels to respond to a naked muon; the error matrix eigenvalues (large semi-axes of error ellipsoids) as obtained from the fit and the angular error σ_θ obtained from the error matrix (with θ being the zenith angle); as well as the exclusion of zero correlation or full correlation between fitted track parameters.

Fig.15 shows a typical single muon event firing 7 of the 18 channels of *NT-36*. It was reconstructed according to the described procedure, with a $\chi^2/NDF = 0.57$.

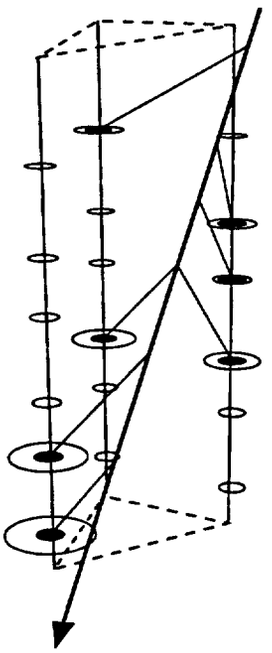

Figure 15: Single muon event recorded with *NT-36*. Hit channels are in black. The thick line gives the reconstructed path, thin lines pointing to the channels mark the path of Cherenkov photons as given by the fit to the measured times. The sizes of the ellipses are proportional to the recorded amplitudes.

Fig.16 shows the distribution of the zenith mismatch angle $\Delta\theta$ as obtained from MC calculations. The long tail with large mismatch angles is substantially lowered by application of the quality criteria. The median zenith mismatch angle for the given set of cuts was obtained to be 7.2° before and 1.8° after application of the quality criteria. The errors for the full spatial mismatch angle are 12.3° and 4.0°, respectively. These values are rather conditional: with stronger cuts the resolution improves but the number of rejected events increases and consequently the effective area decreases. The quality cuts leading to the angular resolution quoted above are passed by 28 % of the downward muons (rejecting most of the muon bundles).

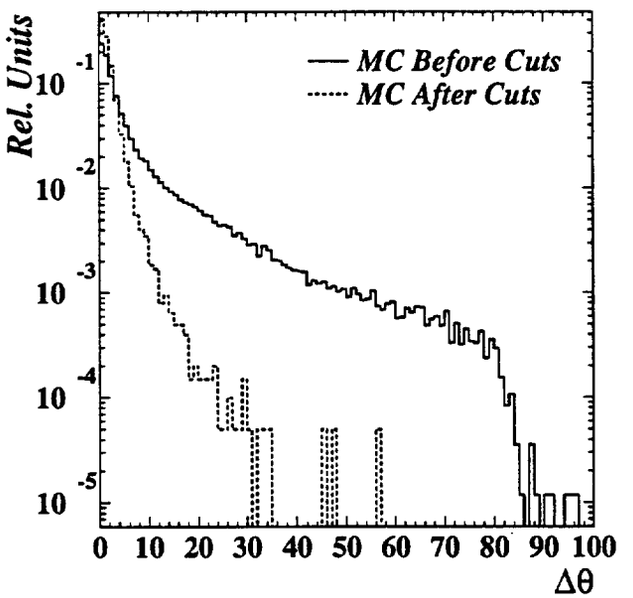

Figure 16: Distribution of the zenith mismatch angle for NT-36 obtained from MC simulations of atmospheric muons.

From the measured angular distribution of events, $N_{exp}(\theta)$, the muon intensity $I_\mu(\theta)$ at the detector depth may be obtained:

$$I(\theta) = \frac{N_{exp}(\theta)}{t_{exp}} \cdot \frac{K_{cut}}{S_{eff}(\theta) \cdot f_{dist}(\theta)}$$

Here, t_{exp} is the data taking time; $S_{eff}(\theta)$ is the effective area of the array as a function of the zenith angle. K_{cut} is the ratio between MC and experimental efficiencies with respect to the applied cuts. It depends only weakly from θ. The distortion function $f_{dist}(\theta)$ is obtained from Monte Carlo calculations and gives the ratio between the number of events *reconstructed* in an interval $\Delta\theta$ around the zenith angle θ and the number of events with their *true* zenith angle in $\Delta\theta$:

$$f_{dist}(\theta) = \frac{N_{rec}(\theta)}{N_{true}(\theta)}$$

$f_{dist}(\theta)$ is close to unity in the interval $0.4 < \cos\theta \leq 1$, but then strongly increases towards smaller $\cos\theta$. This is due to the effect of angular smearing by the reconstruction procedure and the fact that the zenith angle distribution steeply falls towards $\cos\theta = 0$).

The angular distribution $I_\mu(\theta)$ of the muon flux obtained from the equation above is shown in fig.17.

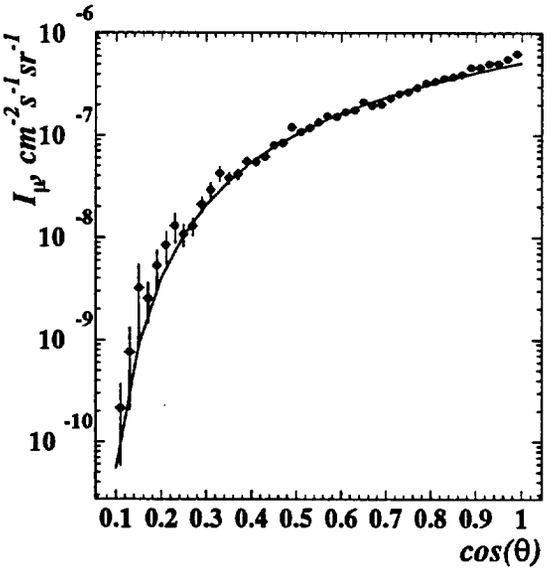

Figure 17: Zenith angle distribution of the muon intensity $I_\mu(\theta)$ at a depth of 1170 m. Full circles: experimental data, solid line: $I_\mu(\theta)$ calculated for stochastic energy loss, respectively [43].

4.5 Depth-intensity relation

The angular dependence of the muon flux $I_{\mu,L_0}(\theta)$ at a given depth L_0, can be transformed into the depth dependence of the vertical flux $I_{\mu,L}(0)$ at different depths $L = L_0/\cos\theta$.

Firstly, the threshold energy of a muon at sea level, $E_{th}(L)$, necessary to punch down to the array under a zenith angle θ (i.e. to pass a water column of thickness $L = L_o/\cos\theta$) is calculated. Using the known angular distribution $I_\mu(\theta, E_{th}(L))$ of the muon flux above a fixed threshold we calculate the ratio

$R = I_\mu(0, E_{th}(L)/I_\mu(\theta, E_{th}(L))$.

The vertical intensity at depth L corresponding to the zenith angle θ is then given by

$I_{\mu,L}(0) = I_{\mu,L_0}(\theta) \cdot R$.

Fig.18 shows a comparison of our results obtained by this procedure with other published values [42] of $I_{\mu,L}(0)$ as well with the dependence calculated in [43].

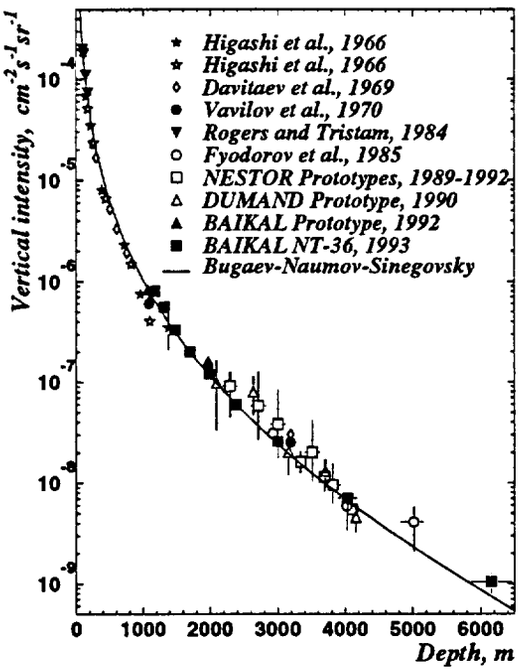

Figure 18: Vertical muon flux, $I_\mu(cos\theta = 1)$, vs. water depth L. The five *NT-36* values (full triangles) are calculated for $\cos\theta =$ 0.2 to 1.0 in steps of 0.1. The other data points are taken from refs.[42]. The curve is taken from [43].

5 Separation of Upward Moving Muons

A first challenge for deep underwater detectors is the identification of upward muons generated in interactions of atmospheric neutrinos. With the flux of downward muons in 1 km depth exceeding that of upward muons from interactions of atmospheric neutrinos by six orders of magnitude, and with the complications of track reconstruction in underwater telescopes described in the previous section, this task appears to be extremely difficult with a detector as small as *NT-36*.

The zenith angle spectrum of events passing the reconstruction procedure outlined in section 4 fits the predicted spectrum from atmospheric muons down to $\cos\theta \approx 0.1$. However, a fraction of $1.5 \cdot 10^{-4}$ of the initial sample of experimental events is reconstructed as upward going muons, in raw agreement with the MC sample. Starting from an initial up-to-down ratio of 10^{-6}, the signal-to-noise ratio S/N of muons from atmospheric neutrinos to fake events is

$$S/N = \frac{0.4}{10^6 \cdot 1.5 \cdot 10^{-4}} \approx \frac{1}{4 \cdot 10^2}$$

Here, 0.4 is the passing rate for neutrino-induced upward muons with the atmospheric neutrino flux generated according to [41].

In order to improve this S/N to the limit given by the small size of *NT-36*, we have developed special "upward-muon" procedures and applied them to the remaining events:

- A track reconstructed as upward track ($\theta > 90°$) is fitted repeatedly with a zero approximation corresponding to a random distribution exponentially in θ. If one of the fits yields a low-χ^2 solution with $\theta < 90°$, the event is rejected from the upward candidate sample.
- There should be at least one hit in one of the upper 6 channels, i.e. in one of the channels of the two upper floors.

  This cut effectively removes events due to showers below the array. The upward traveling light from such shower might fake the time pattern of an upward moving muon. However, the amplitude would fall steeply with increasing height, and in most cases the upper channels would not respond at all.

With the help of the latter criteria, only 26 upward muon candidates out of $2.7 \cdot 10^6$ experimental events fulfilling trigger *6/3* are left. (This numbers relate to the time period when ≥ 16 of the 18 channels have been working.) With a MC passing rate of 21% for neutrino-induced upward muons, this corresponds to

$$S/N = \frac{0.21}{10^6 \cdot (26/2.7 \cdot 10^6)} \approx \frac{1}{45},$$

i.e. the average probability of one of the 26 experimentally upward events to be a true upward muon is about 2%. From the MC muon sample, $S/N = 1/35$ is obtained. Clearly, due to the small number of PMTs and the short lever arm, *NT-36* is not suitable to separate neutrino events. (An exception is a small angular region just around the opposite zenith – see below).

Fig.19 shows an event reconstructed as upward muon and passing all cuts with the exception of the second of the upward muon criterion. The high amplitudes at the bottom of the detector indicate that this event may be due to a shower below the array.

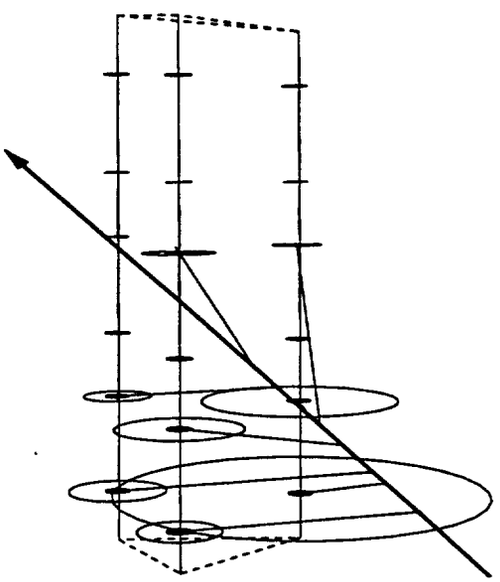

Figure 19: An event recorded with *NT-36*, reconstructed as upward muon and passing all cuts with the exception of the second upward-muon criterion. The time pattern of an upward muon (thick line) is likely to be faked by a shower just below the array yielding large amplitudes in the bottom channels.

Fig.20 shows the $\cos\theta$ distribution for events reconstructed as upward muons and passing the upward-muon cuts. The left distribution contains the 26 events of the experimental sample. The right figure gives the distribution of the MC generated neutrino sample, just after the reconstruction (i.e. without *any* cut) and after upward-muon cuts. The ratio of the lower to the upper distribution is 0.21. As can bee seen, the upward-muon cuts strongly suppress not only fake events but also true upward events close to the horizon.

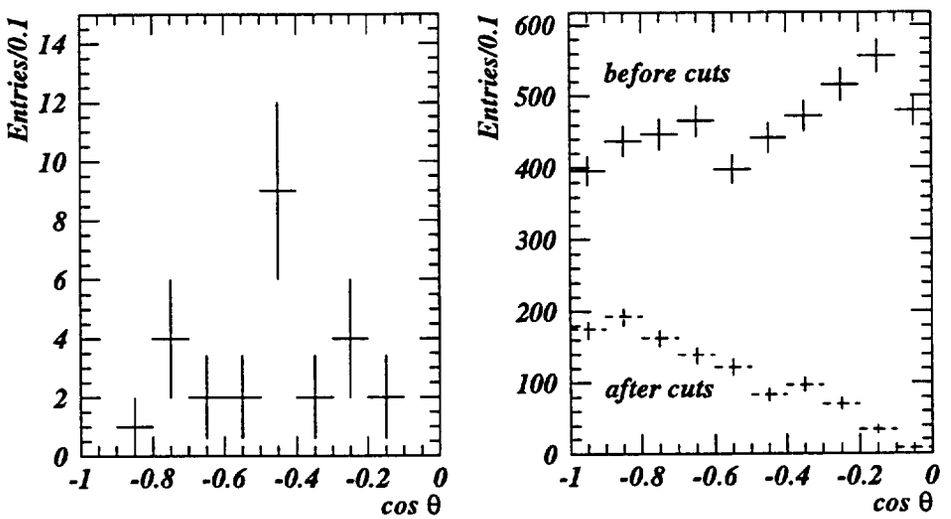

Figure 20: $\cos\theta$ distribution for events reconstructed as upward muons and passing the upward-muon cuts. Left side: experimental data. Right side: MC generated upward muons from interactions of atmospheric neutrinos. Full crosses: after reconstruction, but without any cuts; dashed crosses: after upward-muon cuts.

The approximate agreement of experimental results from *NT-36* with MC simulations gives confidence to believe in the S/N calculated for *NT-200*. In fact, our MC calculations predict a S/N bigger than 1 for *NT-200*. The larger detector allows to loosen considerably some of the cuts which have been extremely tightened for the small *NT-36*. A passing rate of 40-50% for upward muons is obtained for *NT-200*, instead of 21%. Particularly, the acceptance close to the horizon improves dramatically. Moreover, calculations as well as the first data analyzed indicate that already with the 96-PMT array deployed in 1996, a S/N of the order of unity may be obtained.

For muons coming nearly straight upward, S/N should be much better – once due to the noise steeply falling with increasing zenith angle, secondly since the muons have nearly the same orientation like the strings, and an up-down rejection may be achieved even in the case of no full spatial reconstruction, i.e. for events hitting only OMs from 1 string. We have chosen the following criteria to separate nearly vertical upward muons:

- 3 down-facing and at least 1 up-facing channels at one string exclusively must be hit, with time differences between any two hit channels i and j obeying the inequality $|(t_i - t_j) - (T_i - T_j)| < 20ns$, where $t_i(t_j)$ are the measured times, $T_i(T_j)$ are the times expected for minimal ionizing, up-going vertical muons.

- The signals of down-facing channels should be significantly larger than those of upward-facing channels. Any combination of oppositely directed hit channels must obey the inequality $(A_i(\downarrow) - A_j(\uparrow))/(A_i(\downarrow) + A_j(\uparrow)) > 0.3$ with $A_i(\downarrow)$ and $A_j(\uparrow))$ being the amplitudes of channels i and j facing down and up, respectively.
- All signals of down facing channels must exceed a minimum value of 4 *p.e.* (this prevents that the previous cut is dominated by low amplitude events and, consequently, by fluctuations of the few-photoelectron statistics).

We tested the criteria above with the data taken with *NT-36* (April 8, 1994 to March 1, 1995, 212 days of detector life time). Upward-going muon candidates were selected from a total of $8.33 \cdot 10^7$ events recorded during this period by the muon-trigger *3/1*. We found 2 candidates passing our cuts with an expected number of 1.2 events from atmospheric neutrinos as obtained from MC (the samples fulfilling trigger conditions *1*, *1-2* and *1-3* contain 131, 17 and 2 events, respectively). Our preliminary estimates indicate a signal-to-fake ratio $S/N \geq 15$ for these events [44]. A more careful analysis of these neutrino candidates is still underway and will be published elsewhere [45].

6 Search for GUT magnetic monopoles

In 1981, Rubakov [46], and later Callan [47] showed that GUT magnetic monopoles may catalyze baryon decay. For reasonable velocities ($\beta \approx 10^{-4} - 10^{-3}$), a catalysis cross section $\sigma_c = 0.17 \cdot \sigma_o/\beta^2$ is predicted for monopoles crossing water [48], with σ_o being of the order of magnitude typical for strong interactions. This opened a new, although indirect, possibility to detect magnetic monopoles with underwater or underground Cherenkov neutrino detectors. For certain regions of the parameter space in β and σ_o, the Cherenkov light emitted by the decay products would cause sequential hits in individual PMTs in time windows of 10^{-4} - 10^{-3} sec. For large σ_o, "open" detectors like the Baikal telescope can detect monopoles passing very far away – a substantial advantage compared to underground detectors with fixed volume. Corresponding upper limits have been published by our collaboration, using single string arrays [16]. Here we present the limits obtained with *NT-36*.

In the monopole analysis, no use is made of the amplitude and precise arrival time of the PMT pulses, but only of the number of channel hits (local trigger) in a predefined time window variable from 100 μsec up to 8 msec. The coincidence of 2 PMTs not only reduces the 1-PE noise rate of a single PMT to a seasonally dependent value of 50-500 Hz for the local trigger, but also rather effectively suppresses non-Poissonian effects. This can be seen from the results of test runs in which the hits were sampled over a rather long time window (Fig.21). We compare the number of hits detected every 8 msec-time interval, N_{HIT}, with the calculated distribution. The calculation assumes pure Poisson statistics for the hit rate, according to the independently measured average hit rate. Very good agreement with the Poisson assumption is deduced from Fig.21. This agreement is observed for all channels and also for shorter time windows with only very few exceptions.

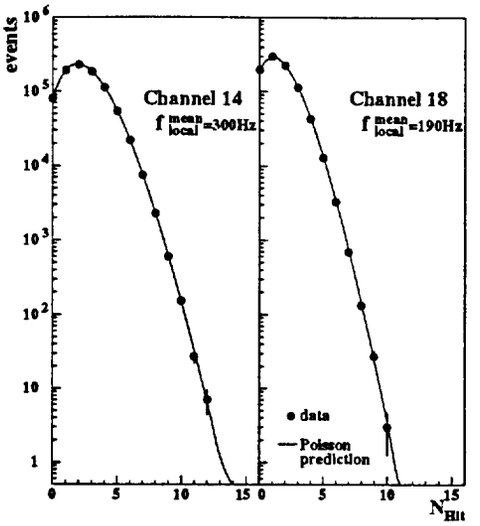

Figure 21: Hit distributions in a time window of 8 msec, as recorded in a 2 hours testrun for channels 14 and 18 of *NT-36*. Experimental data are indicated by points, the curve gives the Poisson prediction.

During standard data taking runs, the monopole trigger condition was defined as ≥ 3 hits within 0.5 msec in any of the channels. With an off-line threshold of 7 hits, one registrates only the uppermost tail of the Poisson distribution. The condition $N_{HIT} \geq 7$ is fulfilled from time to time by pairs with noisy PMTs. To suppress the remaining accidental noise, we defined an even tighter trigger, requesting that *one* PMT pair of a *svjaska* (i.e. a pair of channels oriented face to face) had counted ≥ 7 hits within 0.5 msec, and the other pair 7.5 m away had counted ≥ 3 hits in the same time window. This reduces the number of the experimentally observed monopole candidates to zero. Fig. 22 shows N_{HIT} from the the first pair (channel 1) of a *svjaska* plotted versus N_{HIT} from the face-to-face pair (channel 2). $3.5 \cdot 10^7$ triggers ($N_{HIT} \geq 3$) have been taken from April 16th to November 15th 1993, the product of effective data taking time and number of *svjaska*s with both channels operating is 4573 hours.

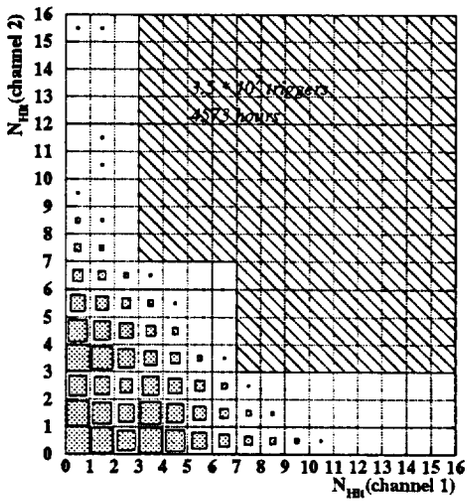

Figure 22: Hit numbers N_{HIT}(chan.2) versus N_{HIT}(chan.1) for all PMT pairs (channels) of a *svjaska*.

Fig. 23 shows the MC calculated effective area for one *svjaska* as a function of the N_{HIT} thresholds in channel 1 and 2 of a *svjaska*, respectively, for different combinations of velocity β and catalysis cross section σ_o. From this, and from the non-observation of any event fulfilling the condition "$N_{HIT}(1,2) \geq 7$ AND $N_{HIT}(2,1) \geq 3$", the flux upper limits (90 % CL) shown in fig. 24 can be derived. We compare the results of the present search with our earlier results and with results published by IMB and KAMIOKANDE [49, 50]. A limit of $5.5 \cdot 10^{-16}$ cm^{-2} s^{-1} has been obtained by the Baksan Telescope for $\beta > 2 \cdot 10^{-4}$ [51]. Our flux limit corresponding to a velocity $\beta = 10^{-4}$ and $\sigma_o = 10^{-29}$ cm^2 is just below the Chudakov-Parker limit [52, 53], for higher cross sections and/or lower velocities it even improves.

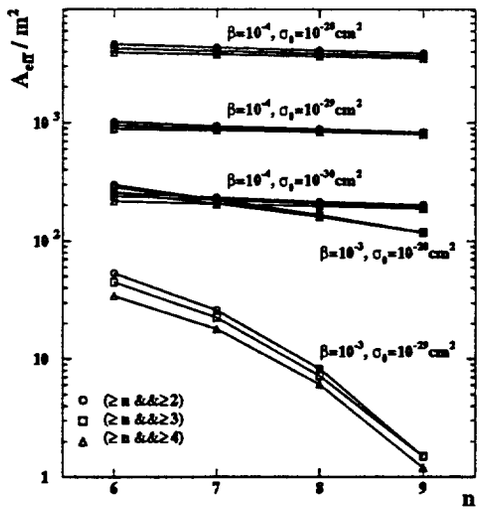

Figure 23: Effective area for a single *svjaska* as a function of the trigger condition "$N_{Hit}(1) \geq n$ AND $N_{Hit}(2) \geq 2, 3, 4$" for different velocities β and catalysis cross sections σ_o.

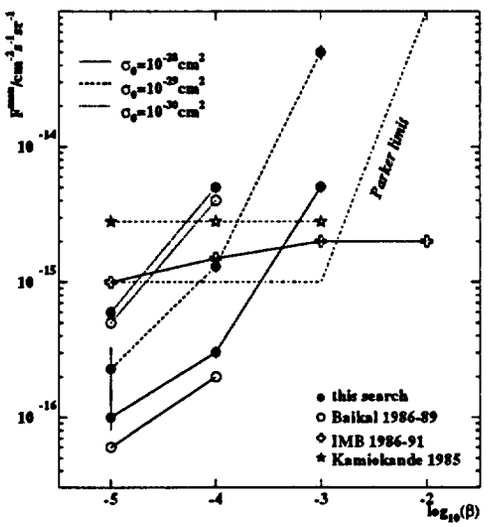

Figure 24: Upper limits (90 % CL) on the flux of magnetic GUT monopoles as a function of their velocity β, for different catalysis cross sections σ_o.

The present analysis uses the same tight trigger condition for all time periods and all channels. This trigger suppresses noise-faked monopole candidates even during periods with high levels of bioluminescence. In the future, it will be tuned corresponding to the average local counting rate of channels. In the case of a positive event, one would try to trace the path of the object through the detector, which should show up by subsequently rising counting rates in OMs along the path.

The counting rate method described above is sensitive not only to monopoles catalyzing baryon decay, but to *any* sufficiently bright object moving with velocities ($\beta \approx 10^{-5} - 10^{-3}$). We have analyzed our data in the framework of GUT monopoles and the Rubakov effect, but could have done the same, e.g., in the less sharply defined framework of quark nuggets [54].

7 Summary and Outlook

We have described the design of the Baikal Underwater Neutrino Telescope *NT-200* and presented methodical and first physics results obtained from the detector *NT-36* installed in April 1993.

The main data stream is due to muons generated in the atmosphere above the detector. Seasonal variations of the water luminescence do not influence the muon trigger rate. The basic characteristics of the muon data like the time differences between different modules, the amplitudes and the distributions of reconstructed muon angles are well reproduced by simulations. Converting the angular dependence into a depth dependence of the vertical flux, good agreement with calculations is observed.

A rejection factor of 10^{-5} for downward muons faking upward muons has been achieved with the small *NT-36* array, the upward-muon passing rate is 21%. With the present analysis method, already a 96-PMT array yields a signal-to-fake ratio of about 1 over most part of the lower hemisphere, with a suppression of only half of the signal events. *NT-200* would do even better. Close to the opposite zenith, even with a 36-OM array neutrino candidates have been separated.

With a special trigger we have searched for slowly moving, bright particles and derived upper limits with respect to GUT monopoles catalyzing baryon decay of the order of the Parker limit.

A major advantage of the site is the existence of a thick ice cover in late winter. Robust deployment and retrieval technologies have been developed using the ice as a stable platform. The displacements of the whole array due to water currents are smaller than 2 m and well monitored by our ultrasonic system. The relative positions of the optical modules do not change by more than 20 cm. Most mechanical components of the system work reliably, particularly none of the modules of *NT-36* did leak. A problem still to be solved is sedimentation on upward facing modules. The initially unsatisfying reliability of some electronics components has been improved considerably over the last 2 years. A 37-cm-diameter hybrid phototube has been developed for the needs of the experiment and produced in more than 250 specimens.

Since April 1996, a four-string array with 96 tubes is taking data. The complete installation of the *NT-200* telescope with 192 tubes and an effective area of about 2000 m^2 is planned for early 1998. Questions that can be tackled with this array include searching for neutrinos from transient cosmic sources like young pulsars formed after a supernova explosion[10], for neutrinos from annihilation of dark matter candidates in the center of the Earth [12, 13], and for magnetic monopoles. Also, the spectra of atmospheric neutrinos and muons will be investigated in detail. On the other hand, theoretical models suggest [9] that only detectors much larger than *NT-200* would be sensitive enough to detect the feeble fluxes from steady astrophysical sources. Therefore, the present Baikal detector is seen last not least as a prototype for a future full-scale telescope. With the deployment and retrieval procedure well under control, the water parameters investigated in detail, the function of the detector as a muon telescope demonstrated and the first neutrino events separated, we have a solid base to envisage this next step. Tentatively, a future large detector might consist of several elongated *NT-200*-like structures [15, 55] of about 300 m height and altogether 2-3 $\cdot 10^3$ optical modules, with an effective area of the order of 10^5 m^2.

Acknowledgments

This project has a long history, and consequently there is a long list of people which helped in various ways to make the experiment alive. First of all we are indebted to M.A.Markov (†) and A.E.Chudakov who contributed basic theoretical and experimental ideas and supported the experiment at all its phases. We also thank V.A.Matveev, V.A.Rubakov, V.Soergel and P. Söding without whose support and patience the last years of development would not have been possible.. We profited from helpful discussions with V.A.Berezinsky, S.P.Mikheyev, A.S.Monin, O.V.Kopelevitch, A.V.Voevodsky, A.G.Zatsepin and G.T.Zatsepin. We express our gratitude to N.A.Airapetova and B.I.Glusman(†) for their invaluable help. We acknowledge the contributions from M.D.Galperin, D.D.Kiss, H.Leich, V.A. Naumov, D.A.Orlov, A.E.Ovchinnikov, L.B.Pavlova, V.A.Poleshuk, V.A. Sevjastonov, P.P.Sherstjankin, L.N.Stepanov, U.Schwendicke and P.Wegner at various stages of the experiment. We thank R.I.Bagduev, B.M.Gluchovskoj (†), G.V. Lisovski, P.A.Putilov and Z.I.Stepanenko for their contributions to the *QUASAR* tube and the optical module, and the Lake Baikal technical staff for their support.

This work was supported in part by the Russian Ministry of Research, the German Ministry of Education and Research, the Volkswagen Foundation, and the International Science Foundation.

References

[1] M.A.Markov, Proc. 1960 Int. Conf. on High Energy Physics, Rochester 1960, 578.

[2] F.Reines, Proc. 1975 Summer Workshop on Neutrino Interactions in the Ocean, Bellingham, Western Washington State College 1976, 5.

[3] L.B.Bezrukov et al., Proc.Int.Conf."Neutrino-84", World Sci. Publ., Singapore 1984, 550.

[4] see e.g. DUMAND-II Proposal, HDC-2-88, Hawaii 1988; A.Roberts, Rev.Mod.Physics 64 (1992) 259.

[5] D.M.Lowder et al., Proc. 23rd ICRC, Calgary 1993, 4, 569; B.Price, Proc. 7th Int. Workshop on Neutrino Telescopes, Venice 1996, 383.

[6] see e.g. L.K.Resvanis (ed.) Proc. 2nd NESTOR-Workshop, Pylos 1992, Univ. Athens (1993).

[7] A.Mazure et al., Test de faisabilité d'un détecteur de neutrinos cosmiques, Letter of Intent, Marseille 1996.

[8] M.Punch et al., Nature 358 (1992) 477.

[9] see the recent reviews V.S.Berezinsky, Nucl.Phys. (Proc.Suppl.) B31 1993) 413; P.Lipari, Proc 23rd ICRC, Calgary 1993; T.K.Gaisser, F.Halzen and T.Stanev, Phys.Rep. 258 (3) (1995) 173; R.Protheroe, Nucl. Phys. B (Proc.Suppl.) 43 (1995) 229; and references therein.

[10] V.S.Berezinsky, Nucl.Phys.(Proc.Suppl.) B31 (1993) 413.

[11] for a review, see G.J.Fishman and C.A.Meagan, Ann.Rev.Astron.Astrophys. 33 (1995) 415.

[12] A.Bottino et al, Astroparticle Physics 3 (1995) 65.

[13] V.Berezinsky et al., CERN-TH 96-42 (E-preprint LANL hep-ph/9603342) and references therein.

[14] A.E. Chudakov, Talk given at the DUMAND Summer Workshop, Khabarovsk/Lake Baikal, 1979.

[15] I.A.Sokalski, Ch.Spiering (eds.), The Baikal Neutrino Telescope, Project Description, Baikal-Report 92-03, Zeuthen 1992.

[16] L.B.Bezrukov et al., Sov.J.Nucl.Phys., 52 (1990) 54.

[17] L.B.Bezrukov et al., Proc.3rd NESTOR Workshop, Pylos 1993, Univ. Athens 1994, 645.

[18] L.B.Bezrukov et al., Oceanology, 28 (1988) 331.

[19] I.A.Belolaptikov et al., Proc. XXVI Int. Conf. High Energy Physics, Dallas (1993) 1246.

[20] V.I.Dobrynin et al., Soviet J. of Chem. Physics, 9 (1990) 212.

[21] B.A.Tarashanski et al., Atmos. and Oceanic Optics, 7 (1994) 818.

[22] O.N.Gaponenko et al., Atmos. and Oceanic Optics, 9 (1996) 677.

[23] I.A.Belolaptikov et al., Proc. 24rd ICRC, Rome 1995, 1 1043.

[24] P.Askebjer et al., Science, 267 (1995) 1147.

[25] A.Roberts, La Jolla, Scripps Inst. of Oceanography, 1 (1979) 139.

[26] A.I.Panfilov, Proc. Techn. Conf. on Ocean and Marine Engineering, Shipbuilding and Maritime Technology, Varna 1992, 36.

[27] I.A.Belolaptikov et al., Proc. 24th ICRC, Rome 1995, 1, 1001.

[28] see e.g. J.Learned, Nucl.Phys.B (Proc.Suppl.) 38 (1995) 484; S.Barwick, Nucl.Phys.B (Proc.Suppl.) 43 (1995) 183; Ch.Spiering, Proc.Int.School "Particles and Cosmology", World Sci.Publ., Singapore 1996, 275; R.Wischnewski, Proc.Int.Europhys.Conf.on High Energy Physics, World Sci.Publ., Singapore 1995, 540.

[29] I.A.Belolaptikov et al., Proc. 24th ICRC, Rome 1995, 1, 536.

[30] I.A.Belolaptikov et al., Proc.23rd ICRC, Calgary 1993, 4, 581.

[31] L.A.Bezrukov et al., The Optical Module of the Baikal Neutrino Telescope, to be submitted to Nucl. Instr. and Methods

[32] R.I.Bagduev et al., Proc.Int.Conf."Trends in Astroparticle Physics", Teubner, Stuttgart/Leipzig 1994, 132.

[33] H.Heukenkamp et al., Informatik Aktuell, Springer, Berlin 1994, 297.

[34] I.A.Belolaptikov et al., Nucl.Phys. B (Proc. Suppl.) 35 (1994) 290.

[35] I.A.Belolaptikov et al., Proc.3rd NESTOR Workshop, Pylos 1993, Univ. Athens 1994, 213.

[36] S.N.Boziev et al., INR Preprint P-0630, Moscow 1989.

[37] S.Ahlen et al., Nucl.Instr. and Meth A234 (1993) 337.

[38] M.M.Boliev et al., Proc. 3rd Int.Workshop on Neutrino Telescopes, Venice 1991, 235.

[39] K.S.Hirata et al., Phys.Rev.D38 (1988) 448.

[40] I.A.Belolaptikov et al., Nucl.Phys B (Proc.Suppl.) 35 (1994) 301.

[41] L. Volkova, Sov.J.Nucl.Phys 31 (1980) 784.

[42] Data taken from: E.G.Anassontzis et al., Proc.23rd ICRC 4 (1993) 554 and Proc. Workshop on High Energy Neutrino Astrophysics, Hawaii (1992) 325 (*NESTOR*); J.Babson et al., Phys.Rev.D42 (1990) 3613 (*DUMAND*); R.Wischnewski et al., Proc.XXVI Int.High Energy Physics Conf., Dallas, USA (1993),1246 (*BAIKAL-Prototype*), S.Higashi et al., Nuov.Cim.43A (1966) 334; L.Davitaev et al., Act.Phys.Acad.Sci.Hung.29 (1969) 53; Yu.Vavilov et al., Bull.Acad.Sci.USSR, Phys.Ser.34 (1970) 1759; I.W.Rogers and M.Tristam, Nucl.Phys.10 (1984) 983; V.Fedorov et al., Proc.19th ICRC 8 (1985) 39.

[43] E.Bugaev et al., Proc.3rd NESTOR Workshop, Pylos 1993, Univ. Athens 1994, 268.

[44] L.B.Bezrukov et al., Proc. 2nd Workshop on The Dark Side of the Universe, World Sci.Publ., Singapore 1996, 221, and E-preprint LANL astro-ph/9601161.

[45] L.A.Bezrukov et al., Separation of nearly vertical upward going muons from neutrino interactions with the Baikal Neutrino Telescope NT-36, in preparation.

[46] V.A.Rubakov, JETP Lett. 33 (1981) 644.

[47] C.G.Callan, Phys. Rev. D26 (1982) 2058.

[48] J.Arafune, M.Fukugita, Phys. Rev. Lett. 50 (1983) 1901.

[49] R.Becker-Szendy et al., Phys. Rev. D49 (1994) 2162.

[50] M.Fukugita, A.Suzuki (eds.), Physics and Astrophysics of Neutrinos, Springer 1994.

[51] M.Boliev, private communication.

[52] G.V.Domogatsky, I.M.Zhelesnykh, Sov. Journal of Nucl. Phys. 10 (1969) 702.

[53] E.N.Parker, Astrophys. J. 160 (1970) 383; M.S.Turner et al., Phys. Rev. D26 (1982) 1296.

[54] see. e.g. E.Witten, Phys.Rev.D30 (1984) 272; A.De Rujula, CERN-TH.3980/84.

[55] L.B.Bezrukov et al., Proc. 24th ICRC, Rome 1995, 785.